Considering the Existence of Exotic Structure in the Cosmic Microwave Background

Andrew Valentini

Carthage College
Kenosha, Wisconsin

A senior thesis submitted to the Carthage College Physics & Astronomy Department in partial fulfillment of the requirements for the Bachelor of Science Degree in Physics

April 17, 2025

Abstract

In this work, we consider the influence of adding additional structure to the cosmic microwave background's (CMB) power spectrum. The standard cosmological paradigm, called the Lambda Cold Dark Matter (ΛCDM) model, writes the power spectrum for primordial perturbations that ultimately gave rise to the CMB as a simple power law, characterized by two parameters. We introduce additional structure into the CMB by including power spectra for simple fields, specifically a random circle field of uniform radii and a random line field, originally derived from a materials science motivation. We simulate the C_ℓ spectrum generated by both of our power spectrum modifications, quantify the strength of fit to observed CMB data from the Planck satellite, and compute Bayes factors of each to determine if the increased fit that results is significant. We find that both modifications allow for a strengthened fit to the CMB data over the ΛCDM model, but determine that such a fit is not significant. This allows us to conclude that, given our current observational data, it is highly unlikely that a field of random circles with uniform radii or a field of random lines is present in the correlations of the CMB.

1 Introduction

The cosmic microwave background (CMB) has been an incredibly rich resource of observational data for constraining models of the early universe and their parameters. A thorough understanding of the cosmic microwave background gives us a confident picture of the early universe, and may even offer indirect observational evidence of theories of quantum gravity. In the standard cosmological picture, called the Lambda-Cold Dark Matter model, the CMB data is fit well with a very simple set of parameters. This model has been successful in describing our current observations of the CMB, but it could always be the case more complex behavior will be discovered upon a finer observation of this field. It is therefore important to give consideration to models with additional parameters which may later receive theoretical justification for.

In this work, we consider modifications to the standard cosmological model by including effects from power spectra that go beyond the simple power law of ΛCDM, partially motivated by results which have claimed that more complicated structure in the CMB *does* exist [1, 2]. In introducing new models with additional parameters, one should always be sure to justify that such modifications provide an enhancement in fit to observed data above what would be expected from the inherent additional complexity of the model. In this work, we therefore give attention to whether or not the observed CMB data justify these modifications, even if they do result in a better fit than the standard cosmological paradigm.

2 Background Material

Before proceeding to the body of this work, we must define the necessary ingredients. We first define the mathematical tools that will be used for introducing our modifications to the CMB in Section 2.1, briefly cover the relevant cosmological physics in Section 2.2, then close by defining the mathematical tools that will allow us to generate an optimized modification and determine whether or not such a fit is significant enough to make positive claims about the existence of our added complexity in Section 2.3.

2.1 Correlation Functions and Power Spectra

The two point correlation function $\xi_2(\Delta \boldsymbol{r})$ between two points $\boldsymbol{r}$ and $\boldsymbol{r}'$ is defined as the expectation value of the field evaluated at two separate points;

$$\xi_2(\Delta \boldsymbol{r}) = \langle \phi(\boldsymbol{r}) \phi(\boldsymbol{r} + \Delta \boldsymbol{r}) \rangle \,. \tag{1}$$

Given some point $\boldsymbol{r}_0$ in a field $\phi(\boldsymbol{r})$, the two-point correlation function tells you how statistically likely you are to find the same field value at a separate point $\boldsymbol{r}_0 + \Delta \boldsymbol{r}$ above the mean field value. For a completely uncorrelated field with mean field value $\bar{\phi}$, the correlation function becomes[1]

$$\xi_2(|\boldsymbol{r}_i - \boldsymbol{r}_j|) = \langle \phi(\boldsymbol{r}_i) \phi(\boldsymbol{r}_j) \rangle = \delta_{ij} - \bar{\phi}^2.$$

In other words, knowing $\phi(\boldsymbol{r}_i)$ tells us no information about $\phi(\boldsymbol{r}_j)$, which is the definition of an uncorrelated, or a random, field.

In contrast, the two-point correlation function for a completely uniform field ϕ_0 just returns zero, since any point on the field has no statistical correlation to any other point above the mean field value.

The two-point correlation function, expressed in Eq. (1), can be defined using the spatial

[1] See Appendix A for the derivation.

integral definition of the expectation value, which gives us

$$\xi_2(\Delta \boldsymbol{r}) = \frac{1}{V} \int_V \phi(\boldsymbol{r}) \phi(\boldsymbol{r} + \Delta \boldsymbol{r}) \, dx. \tag{2}$$

If we are given a correlation function for a field and instead want to arrive at its power spectrum, which is a tool that tells us how a field's power is distributed over frequency, we take the inverse Fourier transform of (2) to find

$$P(\boldsymbol{k}) = \frac{1}{(2\pi)^3} \int \xi_2(\boldsymbol{r}) e^{i\boldsymbol{k}\cdot\boldsymbol{r}} d^3 r, \tag{3}$$

which is derived in Appendix B.

This expression for the power spectrum is currently expressed in Cartesian coordinates. Since our field of interest, the CMB, is ultimately spherical as will be explained in Section 2.2, we now express the power spectrum in spherical coordinates;

$$P(k) = \frac{2}{(2\pi)^2 k} \int_0^\infty \xi_2(r) \sin(kr) dr, \tag{4}$$

which is derived in Appendix C.

This relationship between a given correlation function and its power spectrum will be crucial to the body of this thesis, as it allows us to arrive at power spectra in spherical coordinates from known correlation functions.

2.2 Cosmological Physics and the Cosmic Microwave Background Radiation

The theory of cosmic inflation, the leading class of models that describe the very early phase of our universe's development[2], was originally posed in 1981 [3] as an alternative to the standard big bang model, motivated by the standard theory's flaws that become present when one extrapolates it back to very early times. Inflationary cosmology posits that the early universe underwent a period of exponential expansion driven by the dynamics of a scalar field $\phi(\boldsymbol{r}, t)$, called the inflaton. Under inflation, the scale of the universe increased by an enormous amount during this very early period, expanding by a factor of 10^{50} times greater than what is predicted by the standard big bang model [7].

Inflationary cosmology tells us that the inflaton field $\phi(\boldsymbol{x}, t)$ began as a quantum field, subject to quantum fluctuations. These fluctuations, in combination with a repulsive gravitational force, is ultimately what gave rise to our universe under inflation. Quantum fluctuations normally exist on imperceptible scales, but through the mechanism of inflation, these primordial fluctuations were rapidly stretched to astronomical scales, eventually being "frozen in" as classical density perturbations $\delta\rho(\boldsymbol{x})$ which formed the seeds for cosmic structure and the later development of life.

The first light released from the universe, called the cosmic microwave background radiation (CMB), was first serendipitously discovered in 1964 by Arno Penzias and Robert Wilson [8] at Bell Telephone Laboratories. Many telescopes and observational facilities have since been built to more precisely measure this radiation, with the first, called the Cosmic Microwave Background Explorer (COBE), telescope launched in 1989 [9]. Although Penzias and Wilson's first observation of the CMB revealed a near perfectly uniform field of radiation, our continued precision in observational measurement of this light has slowly revealed its non-uniformity. We have since discovered that the CMB's radiation follows a Gaussian distribution to a high degree of certainty, though there are theoretical motivations for the

[2]See [3, 4, 5, 6] for foundational papers in the theory of inflation.

radiation to ultimately be non-Gauassian. Fig. 1 demonstrates how the increased precision in CMB measurements have revealed this field's Gaussianity.

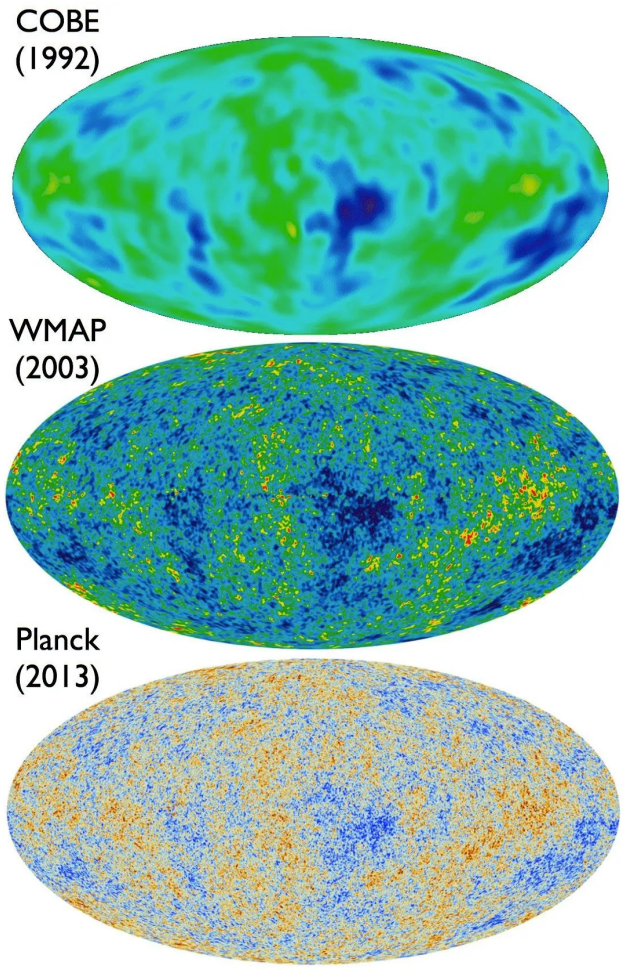

Figure 1: The cosmic microwave background field as measured by COBE in 1990 [10], WMAP in 2003 [11], and the Planck satellite in 2018 [12] demonstrate the slow emergence of this field's Gaussianity. The temperature of the CMB is plotted by color in this figure. Note these maps are spherical, meaning the CMB radiation is the 2D surface formed from a sphere centered around the Earth. These maps are analogous to how the Mercator map projects the Earth's geography onto a 2D plot.

This non-uniformity of the CMB is subject to a great deal of attention in physics and astrophysics, as these fluctuations were ultimately caused by the quantum mechanical nature

of the early universe, which has statistical uncertainly inherently built into its nature. As such, the CMB is our only current observational probe of the early state and development of the universe[3]. When one creates models for the CMB, assumptions of the nature of the early universe's radiation field, and ultimately the nature of inflation, are therefore baked into the models.

To model the CMB, it is standard for one to plot the angular power spectrum C_ℓ as a function of multipole moments ℓ, which describes how the radiation is distributed over different angular scales. The multipole moments ℓ are the angular analog of wavenumbers k, which tell you how many ripples fit on a 360° around the sky.

In this thesis, we will be generating power spectra from known correlation functions. In order to introduce the influence of these power spectra, which live in flat Euclidean space, on the *angular* power spectrum of the CMB, we must use the relationship

$$C_\ell = \frac{4\pi}{(2\pi)^3} \int P(k) j_\ell^2(kr)\ dk, \tag{5}$$

which tells us how to project a power spectrum from flat space onto the surface of a spherical object. This projection is derived in Appendix D.

In standard inflationary cosmology, the power spectrum that generates the CMB fluctuations, called the primordial power spectrum and denoted as $\mathcal{P}(k)$, is modeled as a power law with free amplitude A and spectral index n_s parameters:

$$\mathcal{P}(k) = A_s \left(\frac{k}{k_0}\right)^{1-n_s}. \tag{6}$$

For future relevance, it is important to notice that this power spectrum is unitless. From modern CMB observations, we have determined $A_s = 2.09681 \times 10^{-9}$ and $n_s = .965$ [15].

[3]Though there has been work on what new information and constraints the observation of gravitational waves from this era, called primordial gravitational waves in the literature, would bring. For example, see [13, 14]

2.3 Bayesian Analysis

The Bayesian interpretation of statistics states that the probability of a variable of interest quantifies our uncertainty about it, rather than representing the frequency of specific values of this variable that is taken on, as is the interpretation taken by frequentist statistics. Since probability is a variable's uncertainty under the Bayesian philosophy, it is said to represent a measure of our belief about this variable. In probability being a measure of our knowledge of a variable, it follows that probability is *not* only relies on the result of repeated experiments in which the variable's value is observed, but also includes the effect of what we believe the variable's value to be. In this way, Bayesian statistics allows one to fluidly update their knowledge of a variable upon multiple observations of data that constrain the variable's range of possible values.

Because we often have theoretical predictions for values that variables of interest in physics could take on, it is very common to employ Bayesian methods that make use of these, since they often constrain the space of parameter values. The framework of Bayesian analysis results in a final probability distribution for variables of interest, which is of great interest to physicists. Bayesian statistics is found widely in physics, especially in contexts where observational data is incoming, and models need to be constantly updated in accordance with a continuing observation of data.

Bayes theorem, the foundation of Bayesian statistics, is stated as

$$P(\Theta|D) = \frac{P(\Theta)P(D|\Theta)}{P(D)}. \tag{7}$$

Where $P(\Theta)$, called the *prior* distribution, represents our prior hypothesis about our parameters of interest Θ. When we have no knowledge about our parameters Θ, a constant prior distribution is chosen since this equally weights all possible parameter values.

$P(D|\Theta)$ is called the *likelihood*, which represents the probability of generating the observed

data D given model parameters Θ and is often written as $\mathcal{L}(\Theta)$[4].When measurements made to construct the data are made up of random, independent samples, the central limit theorem is used to state that the likelihood for these processes should be a Gaussian distribution;

$$\mathcal{L}(\Theta) \propto \exp\left(-\sum_i \frac{\left(D_i - M_i\right)^2}{2\sigma_i^2}\right), \tag{8}$$

Because the Planck data provides asymmetric bounds on the uncertainty in C_ℓ, with a lower bound error of $-\delta\ell_i$ and an upper bound error of $+\delta\ell_i$ for every ℓ value in the C_ℓ spectrum, which is the function we ultimately seek to fit, we compute the variance in evidence as

$$\sigma_i^2 = \frac{(+\delta\ell_i)^2 + (-\delta\ell_i)^2}{2}.$$

$P(D)$ is called the *evidence*, which represents the probability of seeing the data under all possible parameter values;

$$P(D) = \int P(D|\Theta)P(\Theta)d\Theta. \tag{9}$$

The evidence acts as a normalizing factor for the posterior distribution. Sampling techniques are especially useful when the model parameters make up a high dimensional space, which makes the integral in Eq. (9) very computationally expensive. A resolution to this problem will be explained shortly when discussing MCMC sampling.

The result of Eq. (7), the *posterior* distribution $P(\Theta|D)$, represents our updated hypothesis about the parameters of interest upon observation of the data. Achieving a distribution for each parameter is the goal of Bayesian statistics, for this tells us which parameter values most likely fit the given data. When the posterior cannot be directly evaluated, it is often approximated using MCMC sampling.

In greater detail, Monte Carlo methods approximate a distribution by using a Markov chain to sample from it. The Markov chain takes a stochastic walk around the distribution

[4]It's crucial to state that the likelihood is *not* a probability distribution for parameter values of Θ. It is a function $f(\Theta)$ that quantifies how well the parameters describe the observed data.

of interest, and therefore approximates its behavior without needing a full analytic expression for it. This Markov chain Monte Carlo sampling technique is used to approximate distributions whose behavior is too difficult to represent analytically or computationally expensive to do so. In the context of Bayesian analysis, MCMC methods are used to approximate the posterior as $P(\Theta|D) \approx P(\Theta)P(D|\Theta)$ since the evidence integral, defined in Eq. (9), can easily become difficult to evaluate given that integrates over all allowed Θ values.

We are allowed to approximate the posterior using MCMC methods, which drop the evidence term, because the sampling technique relies on *relative probability*; how the probability of a randomly chosen point in the $P(\Theta|D)$ distribution looks *compared* to the subsequently chosen values throughout the sampling process whereas in the full expression of Bayes theorem in Eq. (7), $P(D)$ acts as a normalization constant, so the posterior's probabilities are normalized and can be compared in an *absolute* sense.

The final statistical tool to be introduced will allow us to quantify the support for our models that consider the influence of additional structure in the CMB correlation function. In considering models that introduce new parameters to fit data that is already well-fit by more simple models, one must address whether or not the additional parameters are providing any additional fit that can't be explained by just the increased degrees of freedom in the model. This problem of overfitting one's data is a common concern in physics, and the necessary skepticism towards high-parameter models is best captured in John Von Neumann's statement, as relayed by Enrico Fermi [16],

> *"With four parameters I can fit an elephant, and with five I can make him wiggle his trunk."*

To avoid positive conclusions about the ability of our models with additional parameters to better explain the CMB data, we will use another technique commonplace to Bayesian analysis, called the *Bayes factor*. The Bayes factor takes the ratio of two competing models' likelihoods, which will be the standard Lambda cold dark matter model of cosmology and

the added structure models in our case. The Bayes factor therefore looks like:

$$K = \frac{P(D|\Theta_{\rm mod})}{P(D|\Theta_{\Lambda CDM})}. \tag{10}$$

If our models with additional parameters *do* result in a better fit to the data than what is given by ΛCDM that is actually meaningful, the Bayes factor value will be a large number. Any $K > 1$ indicates that $\Theta_{\rm mod}$ will be more preferred by the data than $\Theta_{\Lambda CDM}$. The strength of this support for a given K value is given here

K **Value**	**Strength of Evidence**
$1 - 3.2$	Insignificant
$3.2 - 10$	Substantial
$10 - 100$	Strong
> 100	Decisive

Table 1: Bayes factor confidence levels sorted by their support for $\Theta_{\rm mod}$'s explanatory power as compared to $\Theta_{\Lambda CDM}$.

We will now move on to discussing the logic of this thesis in more detail and introduce the modified power spectra that we will be dealing with.

3 Procedures

This thesis investigates the influence of additional structure to the primordial power spectrum by comparing the resulting C_ℓ spectrum of the CMB with observational data from the Planck satellite, which is openly provided by the Planck Legacy Archive [17]. To include modifications to the primordial power spectrum, we use Eq. (4) to derive the power spectra that result from the addition of modifications from two-point correlation functions studied primarily from a materials science context in the CMB's field. The two-point correlation function has been derived for a variety of random fields, such as those of lines and concentric circles in [18]. After deriving the power spectra that result from these correlation functions, we will construct a total modified primordial power spectrum $P_{\text{tot}}(k) = \mathcal{P}(k) + P_{\text{mod}}(k)$ where $\mathcal{P}(k)$ is the standard primordial power spectrum given in Eq. (6). The Code for Anisotropies in the Microwave Background (`CAMB`) Python package [19] will be used to generate the modified angular power spectra C'_ℓ that result from our power spectra modifications. Given the set of modified angular power spectra that result from this procedure for each added $\xi_2(\Delta r)$ structure, these will then be plotted against the spectrum generated by standard power-law inflationary cosmology in regards to their fit with Planck's data.

To determine the goodness-of-fit for these modifications, we will first carry out a Bayesian analysis on the free parameters of each specific model to find their optimal values. With optimized C_ℓ modifications, a Bayes factor with the ΛCDM model will then be computed to quantify how likely our modifications explain the observed CMB data beyond the strengthened fit that naturally comes from additional free parameters.

To perform Bayesian analysis with the goal of finding the optimal values for the modified spectrum parameters, which are the density of circles ρ and their radii R in the case of the identical circle field, we assume uniform priors on both of these parameters since these parameters are completely original, meaning we have no prior knowledge of what values they should take. We also assume the likelihood follows the exponential distribution given in Eq. (8) because CMB measurements are taken randomly and independently.

Because the likelihood and priors will be computationally evaluated in Python, we use a MCMC sampler rather than additionally computing the evidence integral, as explained in the background section on Bayesian statistics. In this work, the Python package `emcee` will be used to carry out the Monte Carlo sampling portion of this work.

Finally, to determine how likely these modifications to the primordial power spectrum better explain the angular power spectrum of the CMB, the Bayes factor, as defined in Eq. (10), will be computed for each modification.

3.1 Random Uniform Radius Circle Field

Taking the two-point correlation function for a random field of identical circles as derived in [18],

$$\xi_2(r) = \frac{1}{\pi\rho r\sqrt{1-\left(\frac{r}{2R}\right)^2}} \tag{11}$$

where ρ is the density of these circles and R is their fixed radius. Using Eq. (4) to compute the power spectrum of this field in polar coordinates, we find that

$$P_\circ(k) = \frac{1}{(2\pi)^2}\int_0^{2R}\frac{\sin(kr)}{\pi\rho k\sqrt{1-\left(\frac{r}{2R}\right)^2}}dr = \frac{1}{(2\pi)^2}\frac{R}{\rho k}H_0(2kR)$$

where the integral's bounds come from the range of validity for the correlation function to hold and $H_0(2kR)$ is the zeroth-order Struve function.

To generate the modified C_ℓ spectrum, we write the full power spectrum as a sum of the standard power law and the result of the previous expression,

$$P_{\text{tot}}(k) = \mathcal{P}(k) + \frac{1}{(2\pi)^2}\frac{R}{\rho k}H_0(2kR), \tag{12}$$

and input this into CAMB's `set_initial_power_function` function. Notice that because the primordial power spectrum is unitless, our modification must be unitless as well. Since k has units of Mpc^{-1} and R must be linearly proportional to a distance scale, this requires that

ρ be proportional to a distance scale, likely megaparsecs, squared. Taking $R \sim [\text{Mpc}]$, this implies that $\rho \sim [\text{Mpc}^2]$, which is not a physically reasonable quantity of a two-dimensional density. It therefore must be the case that we cannot simply add our modification models and expect the additional cosmological physics that may be necessary in order to make such a move to appear in our models. The *form* of our power spectrum modifications is still important to consider, though, since we are only missing constant factors on the $P_{\text{mod}}(k)$ terms that would fix our unit analysis. The question of whether or not modifications to the primordial power spectrum result in a strengthened, significant fit to observed CMB data is still open, and providing a confident answer to this question could motivate future theoretical work to understand how to incorporate these power spectrum modifications so that cosmological physics is correctly accounted for. We will proceed by assuming that the additional constant factors that are currently missing are absorbed into ρ for reasons that will become clear.

3.2 Random Straight Lines

The correlation function for random straight lines in a field is also derived in [18], which is discovered to be

$$\xi_2(r) = \frac{1}{2\pi\rho r^2}, \tag{13}$$

meaning we will only have one additional parameter when we consider this modification. Computing the corresponding power spectrum, we find

$$P_|(k) = \frac{1}{(2\pi)^2}\frac{1}{\pi\rho k}\int_0^\infty \frac{\sin(kr)}{r}dr = \frac{1}{(2\pi)^2}\frac{1}{\rho k^2}.$$

Our total power spectrum for the straight line field, including the effect of the primordial power spectrum, is then

$$P_{\text{tot}}(k) = \mathcal{P}(k) + \frac{1}{(2\pi)^2}\frac{1}{\rho k^2}. \tag{14}$$

Notice that we are again required to give ρ units of [Mpc^2] in this modification. To reiterate the point that was made in the previous section, we assume that the cosmological that may be absent from the introduction of this modification is absorbed in the ρ factor, primarily motivated by the fact that ρ is required to take on *very* high orders of magnitude in order to produce a reasonable C_ℓ spectrum.

To emphasize this point and demonstrate how our modified power spectra of Eq. (12) and Eq. (14) will affect their resulting C_ℓ spectrum, we plot these spectra along with the standard power-law spectrum in Fig. 2.

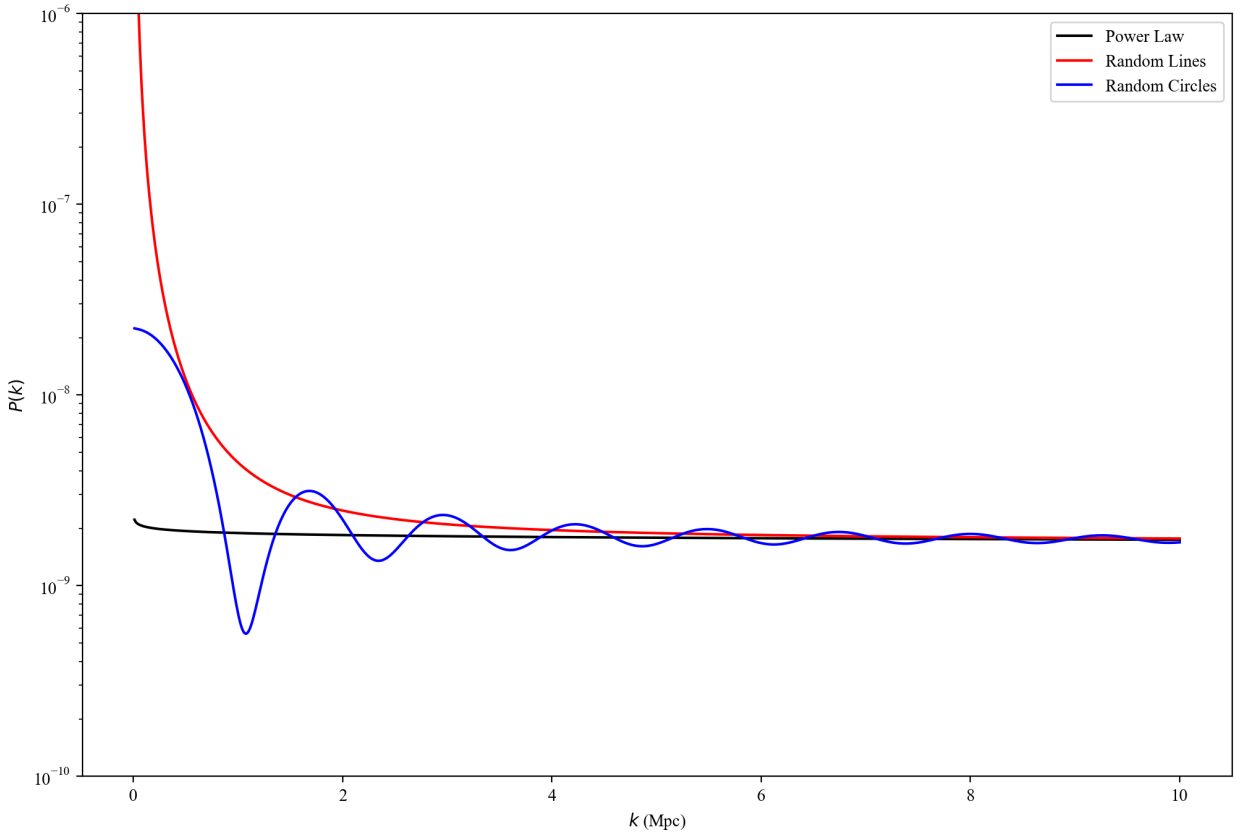

Figure 2: The power spectra generated by our random uniform radius circle and random straight line fields against the standard cosmological power law spectrum. We use $\rho = 1 \times 10^7$ Mpc^2 for both modified power spectra and use $R = 2.5$ Mpc for the random circle field. Note that the low-k oscillations of the random circle field power spectrum become asymptotic at $R \geq 3$ Mpc for our chosen ρ value.

Notice that we have used $\rho = 1 \times 10^7$ Mpc^2 in order to produce Fig. 2. If ρ is not taken to be a value on this scale, we cannot produce a valid C_ℓ spectrum, so we must force incredibly high ρ values which wouldn't make physical sense if ρ were truly representing a valid cosmological density of our circles and lines. This is our primary motivation for assuming that the additional cosmological physics that may be necessary to consider, which is discussed in Section 3.1, is absorbed in our ρ factor.

4 Results

With our modified power spectra, we now wish to determine how the resulting C_ℓ spectra compare against observed CMB data. Given values for the Hubble constant H_0, the baryon density parameter $\Omega_b h^2$, the cold dark matter density parameter $\Omega_c h^2$, the reionization optical depth τ, and a valid power spectrum, `CAMB` will generate an angular power spectrum C_ℓ plot that can be directly compared against the observed CMB data from the Planck satellite.

We begin by generating C_ℓ spectra for both of our modifications using values for R and ρ that are randomly chosen, but selected in such a way that `CAMB` actually converges and produces a valid spectrum. These initial guesses begin to demonstrate the behavior of our modified models and is plotted in Fig. 3.

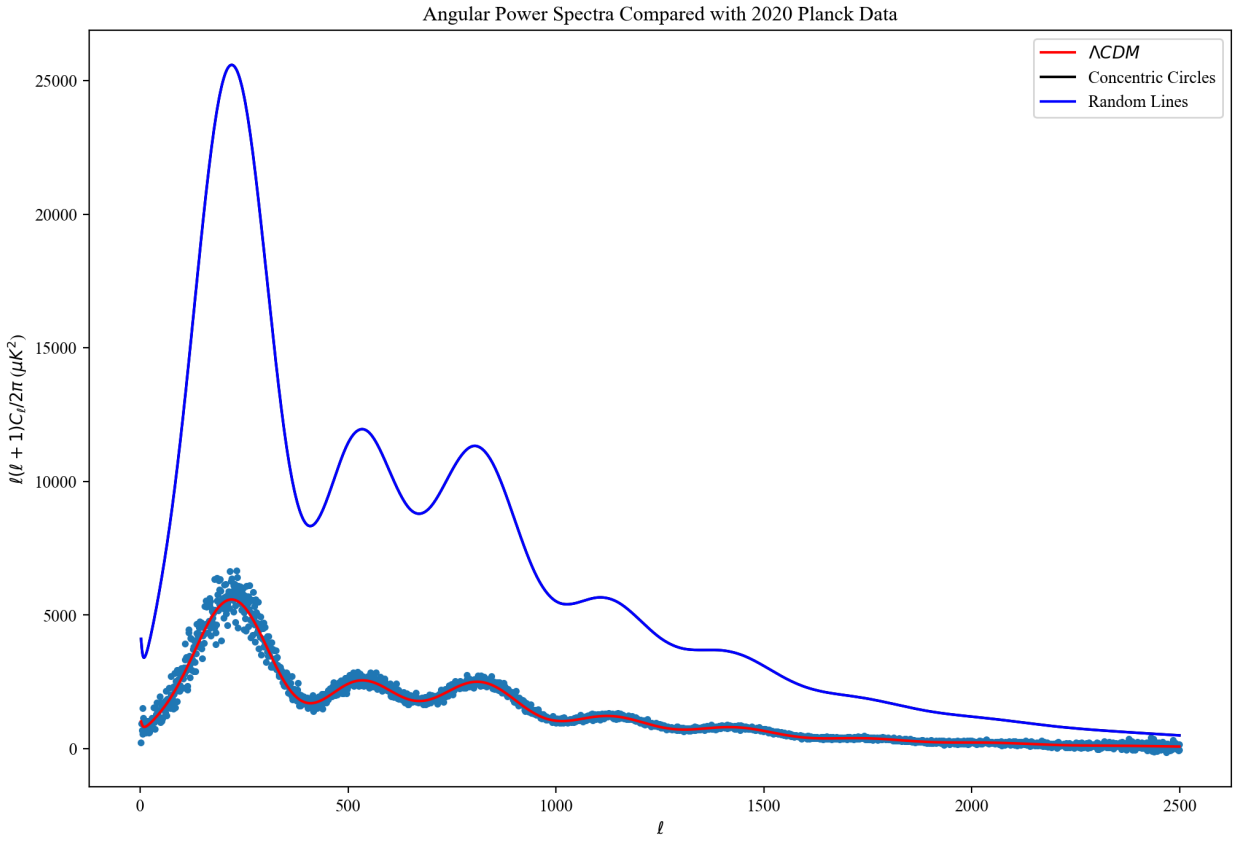

Figure 3: Plotting the resulting C_ℓ spectra for both the random circle and random line field models against the ΛCDM model and the observed spectrum data from the Planck Satellite. Parameters for both modified models were chosen arbitrarily, where $\rho = 1 \times 10^7$ Mpc^2 for both modifications, and $R = 2.5$ Mpc for the random circle model. Note the similarity of the two modified models; they are nearly plotted on top of each other in this figure.

It is clear from Fig. 3 that our modifications seem to match the ΛCDM model and observed CMB data in *shape*, but there is still a vast difference between the *scale* of these models. The following section discusses our process of finding the optimal R and ρ values to begin determining if such modifications better explain the observed data at a level that is statistically significant.

4.1 Results: Random Circle Model

We now wish to find the ρ and R that best fit our data to see if this model results in a better fit over ΛCDM. To do this, we use Bayesian analysis method outlined in Section 2.3 to construct posterior distributions for R and ρ. Carrying this out results in the corner plot for these parameters shown in Fig. 6.

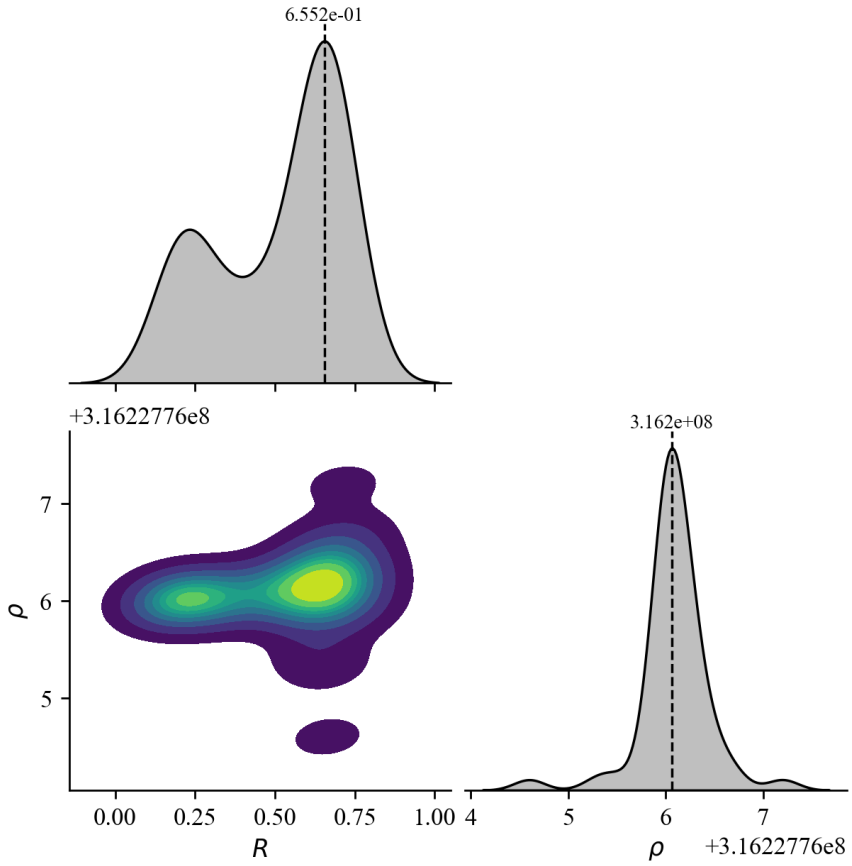

Figure 4: Posterior distributions for R and ρ in the uniform-radius random circle field model. The vertical lines on the marginal distributions represent the most probable values for R and ρ to best fit the observed CMB data, found by the MCMC sampling algorithm.

From the posterior distributions for R and ρ, we take the most probable value for fitting the observed data; the maximum value of the marginal probability distributions. We then use optimized parameters to construct the optimal random circle field C_ℓ spectrum and plot

this against the ΛCDM spectrum and the observed CMB data. Doing so results in Fig. 5

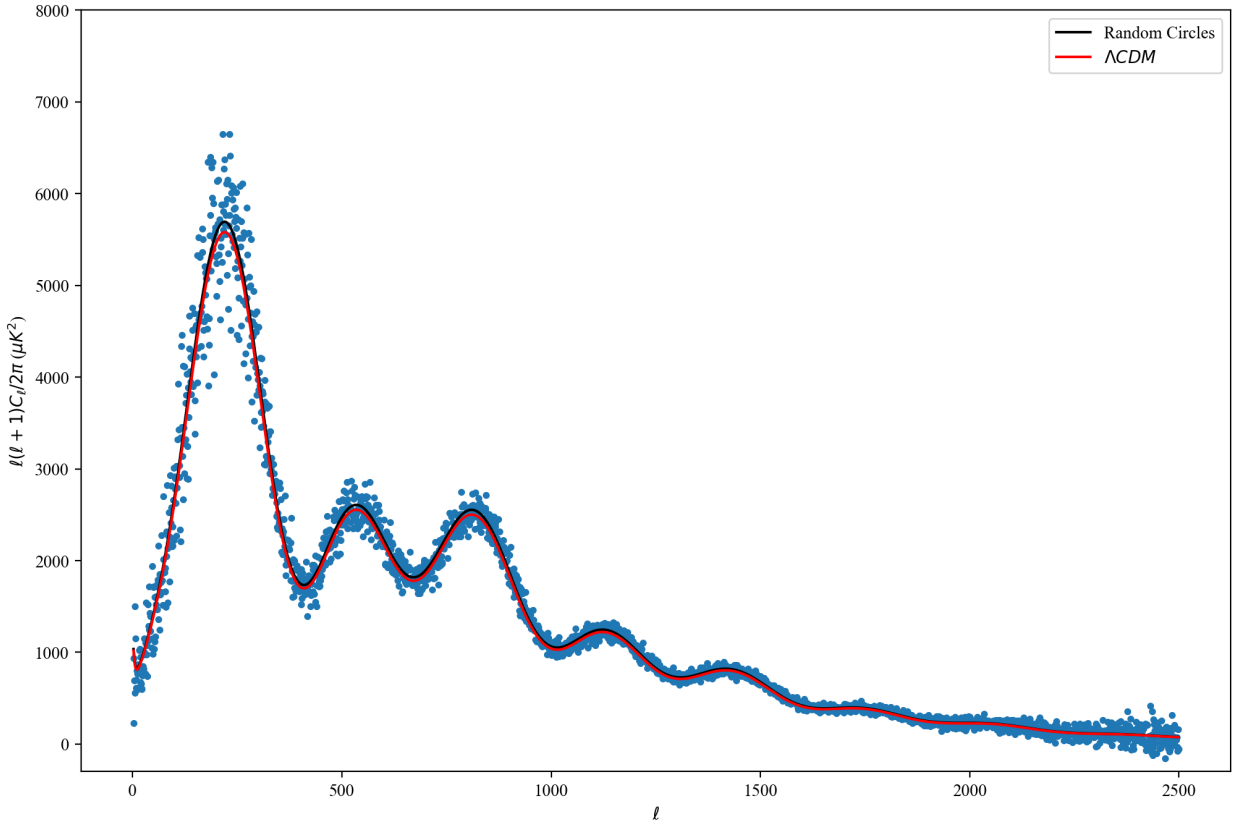

Figure 5: Model generated by optimized $R = .652 \pm .171$ Mpc and $\rho = 3.162 \times 10^8 \pm 1038$ Mpc^2 values for the random circle field plotted against LCDM model and Planck CMB C_ℓ data.

It appears that our random circle model fits the Planck data better than the ΛCDM model, especially when it comes to the first peak in the spectrum. To quantify the alignment of our random circle model in comparison to the ΛCDM model, we compute a χ^2 statistic for both, which is the exponential term of Eq. (8), and compare the two. In doing so, we find that

$$\frac{\chi^2_{\text{circ}}}{\chi^2_{\Lambda CDM}} = .9301,$$

which tells us that our random circle model *does* fit the data better than ΛCDM when its R and ρ parameters are optimized. Discussion of this result and determining the statistical

significance of this result follows in Section 5.

4.2 Results: Random Line Model

To examine the strength of our random line model, we carry out the same procedure as with the random circle model for determining the optimal parameters for fitting the CMB data, although we are now dealing with a model with only one additional parameter, ρ. Constructing a posterior distribution on ρ for the random line model and approximating this using MCMC sampling, we find

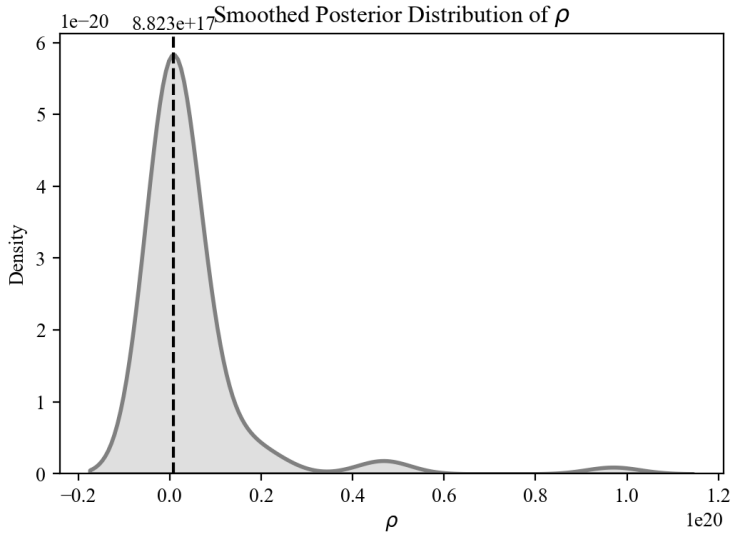

Figure 6: Posterior distribution for ρ in the random line model.

Using the optimal ρ value for our random line model, we again plot the resulting C_ℓ spectrum against the ΛCDM model and Planck data, resulting in Fig. 7

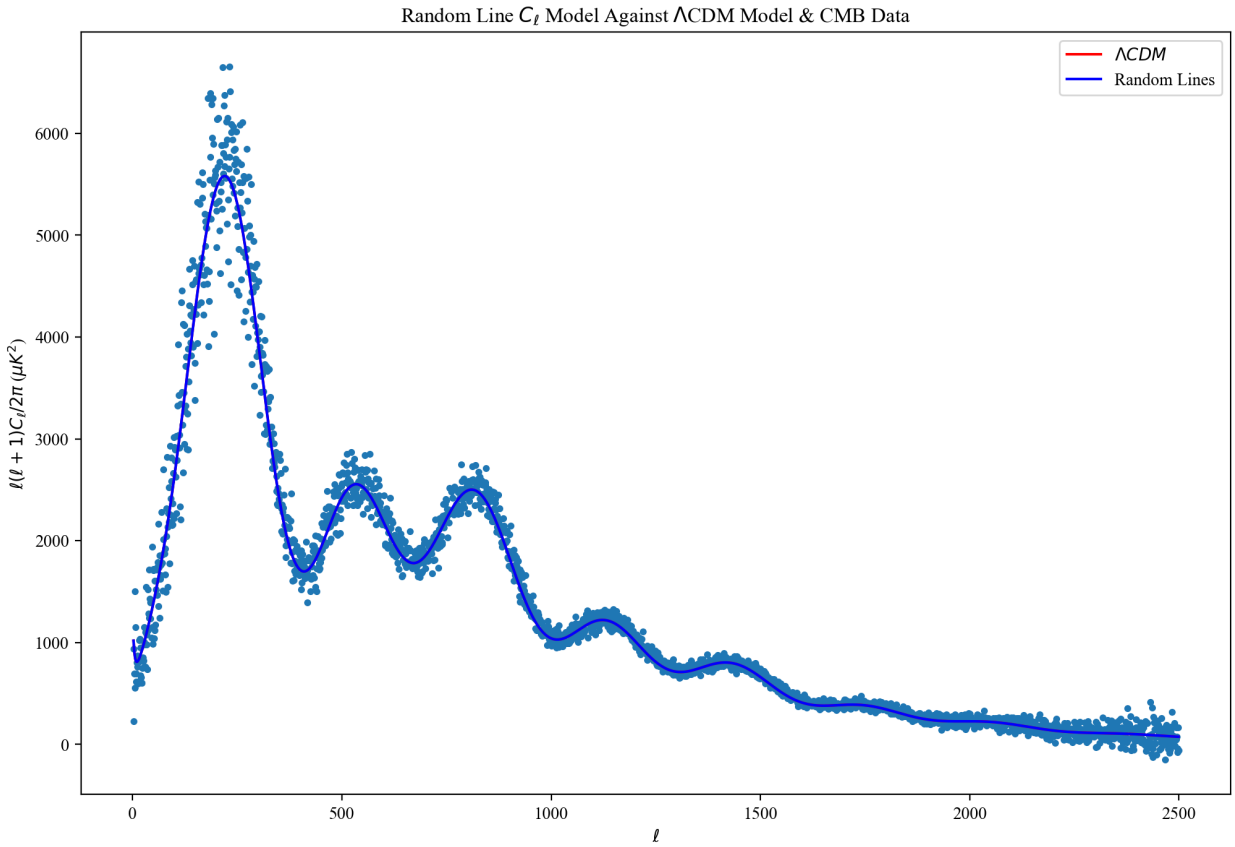

Figure 7: Model generated by optimized $\rho = 3.162 \times 10^8 \pm 1038$ Mpc^2 value for the random line field plotted against ΛCDM model and Planck CMB C_ℓ data. The random lines model has been made nearly identical to the ΛCDM model, and the overlapping of these spectra is present in this figure, as the ΛCDM model is hidden behind the random lines model.

We again compute a χ^2 factor for this modification and compare it with that of ΛCDM. In doing this, we find that

$$\frac{\chi^2_{\text{lines}}}{\chi^2_{\Lambda CDM}} = .999$$

The interpretation of this result will be explained in the following section.

5 Discussion

We have shown that for both the random circle and random line field models, their resulting C_ℓ spectra align with observed CMB data better than the standard ΛCDM model. As was explained in Section 2.3, however, these models should be *expected* to result in an improved fit on account of their additional free parameters. A model with additional parameters should always be expected to provide a stronger fit to data than one without. To determine if the increase in fit to the CMB of our modifications is statistically significant or not; if the additional fit is or is not just due to our free introduced parameters R and ρ and something that may be physically significant, we now compute Bayes factors for both models. Doing so results in the K values recorded in Table 2.

	Random Circles	**Random Lines**
χ^2	.9301	.999
K	2.482	2.718

Table 2: Results table

When comparing the resulting Bayes factor values with Table 1, we quickly conclude that although both of our models are able to fit observed CMB data better than the ΛCDM model is capable of, this strengthened fit is insignificant. We can therefore conclude that the additional fit of these modifications tell us nothing about how robust the motivating physical principles behind them are. This is all to say that neither modification explains the CMB better than the more simple ΛCDM model, and we can therefore conclude that these more exotic structures in the CMB *do not* exist.

These conclusions make a good deal of sense when considering the optimal ρ values for both models, especially for the random line model. In both cases, the optimal fit from these modifications resulted from making ρ extremely large, and since $P_{\text{mod}}(k) \propto \rho^{-1}$ for both models, this essentially neglected the contribution of the modifications to the total power spectrum.

Our Bayes factor results are of some surprise, however, since the additional fit that comes from the random line model is greater than that of the random circle model. One would expect that the oscillations introduced into the random circle power spectrum by the zeroth-order Struve function in Eq. (12) would allow the peaks of the CMB to be better fit. Because the random circle model is reported to result in a better fit to the observed data over the random line model according to each's χ^2 value, the gain in Bayes factor of the random line model could be called into question as just being the result of computational error, especially in the sampling technique used to approximate the posterior distribution for reach model.

Although we have determined that neither modifications result in significant fits to CMB data, the optimized radius parameter value of the random circle field deserves some attention before moving on to the conclusions of this work because it corresponds to a reasonable cosmological scale. To give a sense of our optimized R value of .652 Mpc, the universe had a radius of 42 million light years [20], which corresponds to 12.87 Mpc, at the time of the CMB.

6 Conclusion

We have considered the effect of including additional structure in the CMB's power spectrum, focusing on the addition of random circle and random line fields. We have shown that such modifications do result in a strengthened fit to CMB data, but such an increased fit has been shown to not be significant beyond what is expected from the addition of free parameters R and ρ in our models.

A direction for future work would be considering the influence of a random circle field where the radii of the circles are not constant, as we have considered in this work. Doing so would introduce a probability distribution over the possible radii values for each circle in the field to be sampled from, and a correction function for such a field has been derived in [18].

Suggesting to determine how to make our modifications correctly incorporate cosmological physics so that our density parameter carries the proper units and so that it has a more reasonable value would be another direction of future research, but because we have shown these models offer no significant improvement in fit to the CMB data, such a research direction will not be productive. We proceeded in this work while accepting the glaring problem with our density parameter because the goal of this work was primarily to determine whether or not we could find any reason to support the belief that the CMB's power spectrum does, in fact, require modifications beyond the simple power law of ΛCDM. Because we proceeded without giving attention to the cosmological physics that must necessarily be at play and assumed such corrections would ultimately be absorbed into our ρ factor, our results confidently tell us that pursuing research in this direction will not be productive no matter what the additional cosmological constants look like that eventually become separated out of ρ, at least given our current observation of the CMB. If we had attempted to import the proper cosmological physics early on, this might not have allowed us to make such a general claim as *any model with random circle or random line field modifications to the CMB power spectrum is not supported by current CMB data*.

References

[1] R. Penrose. *Cycles of Time: An Extraordinary New View of the Universe*. Knopf Doubleday Publishing Group, 2011. ISBN: 9780307596741.

[2] V. G. Gurzadyan and R. Penrose. *Concentric circles in WMAP data may provide evidence of violent pre-Big-Bang activity*. 2010. eprint: 1011.3706 (astro-ph.CO).

[3] Alan H. Guth. "Inflationary Universe: A Possible Solution to the Horizon and Flatness Problems". In: *Phys. Rev. D* 23 (2 Jan. 1981), pp. 347–356.

[4] A.D. Linde. "A New inflationary Universe Scenario: A Possible Solution of the Horizon, Flatness, Homogeneity, Isotropy and Primordial Monopole Problems". In: *Physics Letters B* 108.6 (1982), pp. 389–393.

[5] A.D. Linde. "Chaotic inflation". In: *Physics Letters B* 129.3 (1983), pp. 177–181.

[6] Andreas Albrecht and Paul J. Steinhardt. "Cosmology for Grand Unified Theories with Radiatively Induced Symmetry Breaking". In: *Phys. Rev. Lett.* 48 (17 Apr. 1982), pp. 1220–1223.

[7] Stephen Hawking and Werner Israel. "300 Years of Gravitation". In: (1987).

[8] A. A. Penzias and R. W. Wilson. "A Measurement of Excess Antenna Temperature at 4080 Mc/s." In: 142 (July 1965), pp. 419–421.

[9] J. Mather et al. "A Preliminary Measurement of the Cosmic Microwave Background Spectrum by the Cosmic Background Explorer (COBE) Satellite". In: 354 (May 1990), p. L37.

[10] G. Smoot et al. "Structure in the COBE Differential Microwave Radiometer First-Year Maps". In: 396 (Sept. 1992), p. L1.

[11] C. L. Bennett et al. "First-Year Wilkinson Microwave Anisotropy Probe (WMAP) Observations: Preliminary Maps and Basic Results". In: *The Astrophysical Journal Supplement Series* 148.1 (Sept. 2003), pp. 1–27.

[12] Y. Akrami et al. “Planck 2018 Results: VII. Isotropy and Statistics of the CMB”. In: *Astronomy and Astrophysics* 641 (Sept. 2020), A7.

[13] Arthur Kamionkowski Marc Kosowsky and Albert Stebbins. “A Probe of Primordial Gravity Waves and Vorticity”. In: *Phys. Rev. Lett.* 78 (11 Mar. 1997), pp. 2058–2061. URL: https://link.aps.org/doi/10.1103/PhysRevLett.78.2058.

[14] Latham A. Boyle and Paul J. Steinhardt. “Probing the Early Universe with Inflationary Gravitational Waves”. In: *Phys. Rev. D* 77 (6 Mar. 2008), p. 063504. URL: https://link.aps.org/doi/10.1103/PhysRevD.77.063504.

[15] Planck Collaboration. “Planck2018 Results: VI. Cosmological Parameters”. In: *Astronomy amp; Astrophysics* 641 (Sept. 2020), A6. ISSN: 1432-0746. DOI: 10.1051/0004-6361/201833910. URL: http://dx.doi.org/10.1051/0004-6361/201833910.

[16] Freeman Dyson. “A Meeting with Enrico Fermi”. In: *Nature* 427 (2004), p. 297. URL: https://www.nature.com/articles/427297a.

[17] European Space Agency. *Planck Legacy Archive*. https://pla.esac.esa.int. 2020.

[18] H. Stoyan and D. Stoyan. “Simple Stochastic Models for the Analysis of Dislocation Distributions”. In: *Physica Status Solidi (A)* 97.1 (1986), pp. 163–172.

[19] Antony Lewis and Anthony Challinor. *CAMB: Code for Anisotropies in the Microwave Background*. Astrophysics Source Code Library, record ascl:1102.026. Feb. 2011.

[20] David W. Hogg. *Distance measures in cosmology*. 2000. arXiv: astro-ph/9905116 [astro-ph]. URL: https://arxiv.org/abs/astro-ph/9905116.

[21] Florent Leclercq. *Bayesian large-scale structure inference and cosmic web analysis*. 2015. arXiv: 1512.04985 [astro-ph.CO]. URL: https://arxiv.org/abs/1512.04985.

A Two-Point Correlation Function of Uncorrelated Field

Using Eq. (2)

$$\xi_2(|\boldsymbol{r}_i - \boldsymbol{r}_j|) = \frac{1}{V}\int (\phi(\boldsymbol{r}_i) - \bar{\phi})(\phi(\boldsymbol{r}_j) - \bar{\phi}) d^3x$$

When this is expanded and the fact that integrating over the whole field, scaled by its volume returns the mean field value;

$$\bar{\phi} := \frac{1}{V}\int \phi(\boldsymbol{r}_i) d^3x,$$

we get

$$\xi_2(|\boldsymbol{r}_i - \boldsymbol{r}_j|) = \frac{1}{V}\int \phi(\boldsymbol{r}_i)\phi(\boldsymbol{r}_j) d^3x - \bar{\phi}^2. \tag{15}$$

Because the field is uncorrelated, the expectation value of the field at two separate points will always return zero, giving us

$$\xi_2(|\boldsymbol{r}_i - \boldsymbol{r}_j|) = \delta_{ij} - \bar{\phi}^2.$$

B Fourier Transform of Two-Point Correlation Function:

Take Fourier transform

$$\phi(\boldsymbol{r}) = \frac{1}{(2\pi)^3}\int \phi(\boldsymbol{k}) e^{i\boldsymbol{k}\cdot\boldsymbol{r}} d^3k \tag{16}$$

So if we define $\boldsymbol{r}' = \boldsymbol{r} + \Delta\boldsymbol{r}$, we get

$$\xi_2(\Delta\boldsymbol{r}) = \langle\phi(\boldsymbol{r})\phi(\boldsymbol{r}+\Delta\boldsymbol{r})\rangle = \left\langle \frac{1}{(2\pi)^3}\int \phi(\boldsymbol{k}) e^{i\boldsymbol{k}\cdot\boldsymbol{r}} d^3k \frac{1}{(2\pi)^3}\int \phi(\boldsymbol{k}') e^{-i\boldsymbol{k}'\cdot(\boldsymbol{r}+\Delta\boldsymbol{r})} d^3k' \right\rangle \tag{17}$$

using the fact that $\xi_2(\Delta\boldsymbol{r})$ is a real-valued function, which requires the complex conjugate

to be taken of the $\mathscr{F}\{\phi(\boldsymbol{r}+\Delta\boldsymbol{r})\}$ term.

Using the Wiener-Khinchin Theorem for random variables in 3D, $\langle\phi(\boldsymbol{k})\phi(\boldsymbol{k}')\rangle = (2\pi)^3\delta^3(\boldsymbol{k}-\boldsymbol{k}')P(k)$ [21], we get

$$\xi_2(\Delta\boldsymbol{r}) = \frac{1}{(2\pi)^3}\int\int \delta^3(\boldsymbol{k}-\boldsymbol{k}')P(k)e^{i\boldsymbol{k}\cdot\boldsymbol{r}}e^{-i\boldsymbol{k}'\cdot(\boldsymbol{r}+\Delta\boldsymbol{r})}d^3k'd^3k. \tag{18}$$

Integrating over the $\delta^3(\boldsymbol{k}-\boldsymbol{k}')$ term results in

$$\xi_2(\Delta\boldsymbol{r}) = \frac{1}{(2\pi)^3}\int P(k)e^{-i\boldsymbol{k}\cdot\Delta\boldsymbol{r}}d^3k. \tag{19}$$

Finally taking the inverse Fourier transform of this expression, we're left with

$$P(k) = \frac{1}{(2\pi)^3}\int \xi_2(\boldsymbol{r})e^{i\boldsymbol{k}\cdot\boldsymbol{r}}d^3r, \tag{20}$$

which tells us how to arrive at a powr spectrum for a field given its correlation function.

C Expressing the Power Spectrum in Spherical Coordinates

Beginning with our three-dimensional expression for the power spectrum in Cartesian coordinates,

$$P(\boldsymbol{k}) = \frac{1}{(2\pi)^3}\int \xi_2(\boldsymbol{r})e^{i\boldsymbol{k}\cdot\boldsymbol{r}}d^3r, \tag{21}$$

we use the typical integration conversion technique,

$$P(k) = \frac{1}{(2\pi)^3}\int_0^\infty\int_0^\pi\int_0^{2\pi} \xi_2(r)e^{i\boldsymbol{k}\cdot\boldsymbol{r}}r^2\sin\theta d\phi d\theta dr. \tag{22}$$

The ϕ integral gives us a factor of 2π, and we use the definition of the dot product in our exponential term:

$$P(k) = \frac{1}{(2\pi)^2} \int_0^\infty \int_0^\pi \xi_2(r) e^{ikr\cos\theta} r^2 \sin\theta d\phi d\theta dr. \tag{23}$$

Using the substitution $u = \cos\theta$ and using the complex exponential definition of $\sin(kr)$, we get

$$P(k) = \frac{1}{(2\pi)^2} \int_0^\infty \xi_2(r) \frac{2\sin(kr)r}{k} dr. \tag{24}$$

D Deriving the Angular Power Spectrum from Initial Fluctuations

$$a_{\ell m} = \int \phi(\boldsymbol{r}) Y^*_{\ell m}(\hat{n}) d\Omega \tag{25}$$

Using the Fourier transform of $\phi(\boldsymbol{r})$

$$a_{\ell m} = \frac{1}{(2\pi)^3} \int \int \phi(\boldsymbol{k}) Y^*_{\ell m}(\hat{n}) e^{i\boldsymbol{k}\cdot\boldsymbol{r}}\ d^3k\ d\Omega \tag{26}$$

Using the plane wave expansion:

$$e^{i\boldsymbol{k}\cdot\boldsymbol{r}} = 4\pi \sum_{\ell=0}^{\infty} \sum_{m=-\ell}^{\ell} i^\ell j_\ell(\boldsymbol{k}\cdot\boldsymbol{r}) Y_{\ell m}(\hat{\boldsymbol{r}}) Y^*_{\ell m}(\hat{\boldsymbol{k}}) \tag{27}$$

where the spherical Bessel function $j_\ell(kr)$ is defined as:

$$j_\ell(kr) = \sqrt{\frac{\pi}{2kr}} J_{\ell+1/2}(kr) \tag{28}$$

$$a_{\ell m} = \frac{4\pi}{(2\pi)^3} \int \int \phi(\boldsymbol{k}) Y^*_{\ell m}(\hat{n}) \sum_{\ell'=0}^{\infty} \sum_{m=-\ell'}^{\ell'} i^{\ell'} j_{\ell'}(\boldsymbol{k}\cdot\boldsymbol{r}) Y_{\ell' m'}(\hat{\boldsymbol{r}}) Y^*_{\ell' m'}(\hat{\boldsymbol{k}})\ d^3k\ d\Omega \tag{29}$$

Using the fact that

$$\int Y^*_{\ell m}(\hat{n}) Y_{\ell' m'}(\hat{n}) d\Omega = \delta_{\ell\ell'}\delta_{mm'}, \tag{30}$$

this gives us

$$a_{\ell m} = \frac{4\pi}{(2\pi)^3} \int \phi(\boldsymbol{k}) \sum_{\ell=0}^{\infty} \sum_{m=-\ell}^{\ell} i^\ell j_\ell(\boldsymbol{k}\cdot\boldsymbol{r}) Y^*_{\ell m}(\hat{\boldsymbol{k}})\ d^3k \tag{31}$$

Now take $\langle |a_{\ell m}|^2 \rangle$, using $\langle \phi(\boldsymbol{k})\phi(\boldsymbol{k}') \rangle = (2\pi)^3 \delta^3(\boldsymbol{k}-\boldsymbol{k}') P(k)$:

$$\left\langle |a_{\ell m}|^2 \right\rangle = \frac{4\pi}{(2\pi)^3} \int\int P(k)\delta^3(\boldsymbol{k}-\boldsymbol{k}') \sum_{\ell\ell'} \sum_{mm'} i^\ell j_\ell(\boldsymbol{k}\cdot\boldsymbol{r}) Y^*_{\ell m}(\hat{\boldsymbol{k}}) i^{\ell'} j_{\ell'}(\boldsymbol{k}'\cdot\boldsymbol{r}) Y_{\ell' m'}(\hat{\boldsymbol{k}'})\ d^3k' d^3k \tag{32}$$

$$\left\langle |a_{\ell m}|^2 \right\rangle = \frac{4\pi}{(2\pi)^3} \int P(k) \sum_{\ell\ell'} \sum_{mm'} i^\ell j_\ell(\boldsymbol{k}\cdot\boldsymbol{r}) Y^*_{\ell m}(\hat{\boldsymbol{k}}) i^{\ell'} j_{\ell'}(\boldsymbol{k}\cdot\boldsymbol{r}) Y_{\ell' m'}(\hat{\boldsymbol{k}})\ d\Omega dk \tag{33}$$

$$\left\langle |a_{\ell m}|^2 \right\rangle = \frac{4\pi}{(2\pi)^3} \int P(k) \sum_{\ell\ell'} \sum_{mm'} i^\ell j_\ell(\boldsymbol{k}\cdot\boldsymbol{r}) i^{\ell'} j_{\ell'}(\boldsymbol{k}\cdot\boldsymbol{r}) \delta_{\ell\ell'}\delta_{mm'}\ dk \tag{34}$$

$$\left\langle |a_{\ell m}|^2 \right\rangle = \frac{4\pi}{(2\pi)^3} \int P(k) \sum_{\ell} \sum_{m} i^{2\ell} j^2_\ell(\boldsymbol{k}\cdot\boldsymbol{r})\ dk \tag{35}$$

Since $i^{2\ell} = 1$,

$$C_\ell = \frac{4\pi}{(2\pi)^3} \int P(k) j^2_\ell(kr)\ dk \tag{36}$$

This tells us that given a power spectrum $P(k)$, we can generate an angular power spectrum $C(\ell)$ using this integral!